Low-redshift compact star-forming galaxies as analogues of high-redshift star-forming galaxies

Y. I. Izotov[1,2], N. G. Guseva[1,2], K. J. Fricke[2,3], C. Henkel[2,4], D. Schaerer[5,6], and T. X. Thuan[7]

[1] Bogolyubov Institute for Theoretical Physics, National Academy of Sciences of Ukraine, 14-b Metrolohichna str., Kyiv, 03143, Ukraine
[2] Max-Planck-Institut für Radioastronomie, Auf dem Hügel 69, 53121 Bonn, Germany
[3] Institut für Astrophysik, Göttingen Universität, Friedrich-Hund-Platz 1, 37077 Göttingen, Germany
[4] Astronomy Department, King Abdulaziz University, P.O.Box 80203, Jeddah 21589, Saudi Arabia
[5] Observatoire de Genève, Université de Genève, 51 Ch. des Maillettes, 1290, Versoix, Switzerland
[6] IRAP/CNRS, 14, Av. E. Belin, 31400 Toulouse, France
[7] Astronomy Department, University of Virginia, P.O. Box 400325, Charlottesville, VA 22904-4325, USA

Received ; Accepted

ABSTRACT

We compare the relations among various integrated characteristics of $\sim$ 25,000 low-redshift ($z \lesssim 1.0$) compact star-forming galaxies (CSFGs) from Data Release 16 (DR16) of the Sloan Digital Sky Survey (SDSS) and of high-redshift ($z \gtrsim 1.5$) star-forming galaxies (SFGs) with respect to oxygen abundances, stellar masses $M_\star$, far-UV absolute magnitudes $M_{\rm FUV}$, star-formation rates SFR and specific star-formation rates sSFR, Lyman-continuum photon production efficiencies ($\xi_{\rm ion}$), UV continuum slopes β, [O III] λ5007/[O II] λ3727 and [Ne III] λ3868/[O II] λ3727 ratios, and emission-line equivalent widths EW([O II] λ3727), EW([O III] λ5007), and EW(Hα). We find that the relations for low-z CSFGs with high equivalent widths of the Hβ emission line, EW(Hβ) $\geq$ 100Å, and high-z SFGs are very similar, implying close physical properties in these two categories of galaxies. Thus, CSFGs are likely excellent proxies for the SFGs in the high-z Universe. They also extend to galaxies with lower stellar masses, down to $\sim 10^6$ $M_\odot$, and to absolute FUV magnitudes as faint as -14 mag. Thanks to their proximity, CSFGs can be studied in much greater detail than distant SFGs. Therefore, the relations between the integrated characteristics of the large sample of CSFGs studied here can prove very useful for our understanding of high-z dwarf galaxies in future observations with large ground-based and space telescopes.

Зависимость масса-металличность для галактик на $z \geq 2$ смещена на 0.3-0.7dex относительно обычных галактик z=0.
Mannucci et al. (2010): зависимость (12+logO/H) – $SFR^{-\alpha}M_*$ при $\alpha = 0.32$ одинакова для SFG на всех z.

Крутой наклон спектра в УФ части и сильные эмиссионные линии в SFG на больших z указывают на наличие массивного звездного населения, производящего ионизующие фотоны в больших количествах. Предполагается, что SFG могут быть основной причиной реионизации Вселенной, с высоким $\xi_{ion} \times f_{esc}(LyC)$.
ξ_{ion} – эффективность производства Ly-continuum.
$f_{esc}(LyC)$ – доля излучения LyC, покидающего галактики.

В исследованиях реионизации Вселенной обычно принимаются значения $\log [\xi_{ion}/Hz\ erg{-}1] \sim 25.2 – 25.3$. Текущие оценки ξ_{ion} для SFG на больших z согласуются с этими значениями (25.3 и даже выше).

Выборка компактных SFG (CSFG):
SDSS DR16
$R_{50} \leq 3$ arcsec в r
EW(Hβ) >∼ 10Å
Галактики с активными ядрами были исключены

-> ∼ 25000 CSFGs на z <∼ 1

CSFGs с большими EW(Hβ) смещены в сторону более высоких [O III]λ5007/Hβ и более низких[N II]λ6584/Hα по сравнению с обычными SFG на z ∼ 1. Зато согласуются с галактиками на больших z!

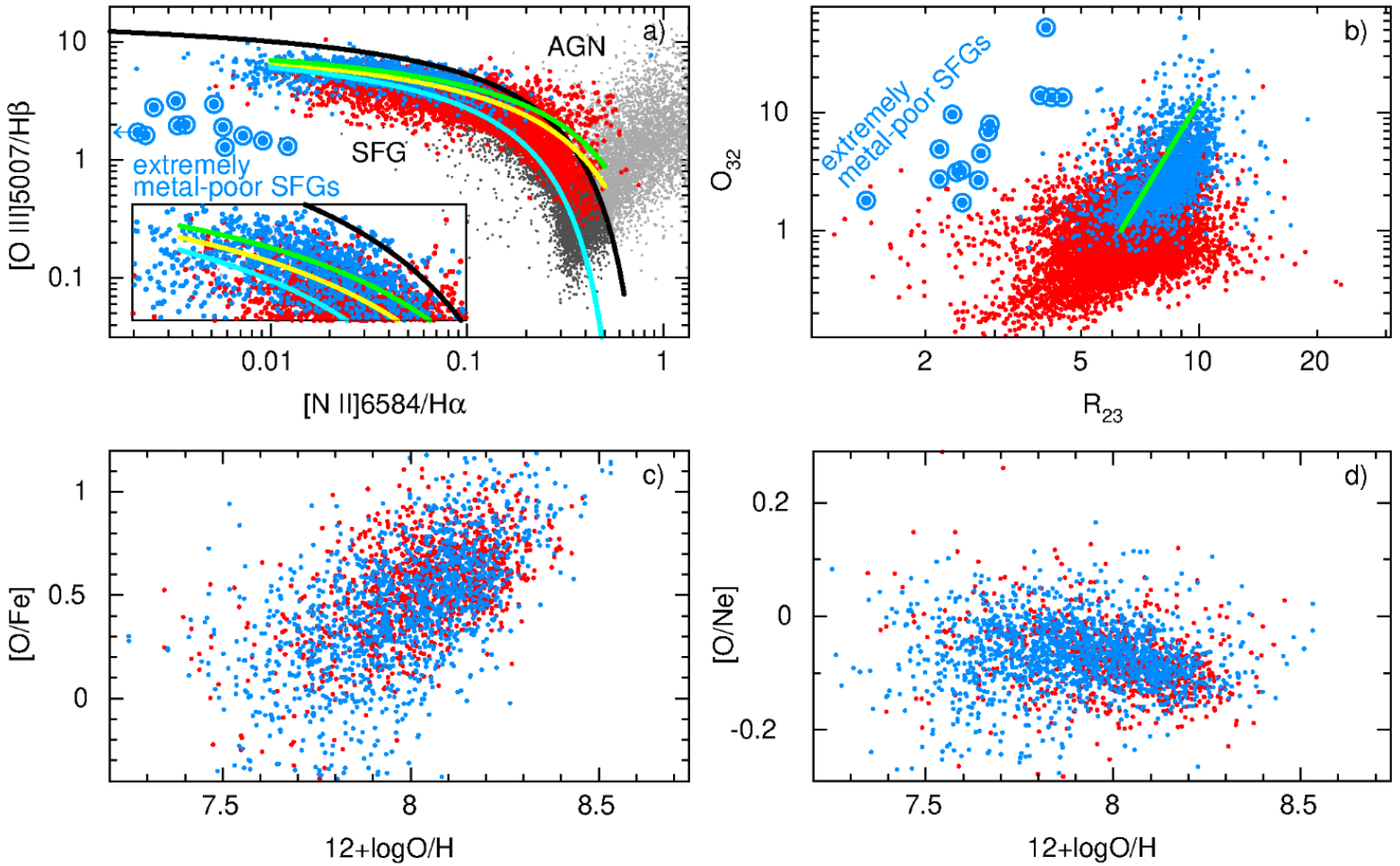

Fig. 1. (a) [O III] λ5007/Hβ vs. [N II] λ6584/Hα BPT diagram (Baldwin et al. 1981) for SDSS DR16 CSFGs with EW(Hβ) ≥ 100Å (blue dots) and with EW(Hβ) < 100Å (red dots). The SDSS DR7 galaxies including both SFGs (without constraints used for selection of CSFGs) and AGN are represented by dark grey dots and light grey dots, respectively. The black line (Kauffmann et al. 2003) separates SFGs from AGN, whereas the cyan line by Kewley et al. (2013) represents the best fit relation for the total sample of $z \sim 0$ SFGs from the SDSS DR7. Yellow and green lines indicate relations for $z \sim 2 - 3$ SFGs by Shapley et al. (2015) and Strom et al. (2017), respectively. An expanded version of the upper part of the diagram in the ranges [N II]λ6584/Hα of 0.006 - 0.16 and [O III] λ5007/Hβ of 4 - 8 is shown in the inset. **(b)** Relation $O_{32} - R_{23}$, where O_{32} = [O III] λ5007/[O II] λ3727, R_{23} = ([O III] λ4959 + [O III] λ5007 + [O II] λ3727)/Hβ. The green line represents the relation for $z \sim 2 - 3$ SFGs by Strom et al. (2017). The most metal-poor nearby galaxies with 12 + log O/H ∼ 6.9 – 7.25 (Izotov et al. 2018c; Kojima et al. 2020, Izotov et al., in preparation) are shown in **(a)** and **(b)** by encircled blue-filled circles. **(c)** Dependence of the oxygen overabundance [O/Fe] ≡ log(O/Fe) – $\log(O/Fe)_\odot$ on the oxygen abundance 12 + logO/H. **(d)** Dependence of [O/Ne] ≡ log(O/Ne) – $\log(O/Ne)_\odot$ on the oxygen abundance 12 + logO/H. Abundances are derived using the T_e method. About ∼ 2300 galaxies with detected [O III]λ4363 emission and an error less than 25% of the line flux are shown in **(c)** and **(d)**. The meanings of the symbols for SDSS galaxies in **(b)** – **(d)** are the same as in **(a)**.

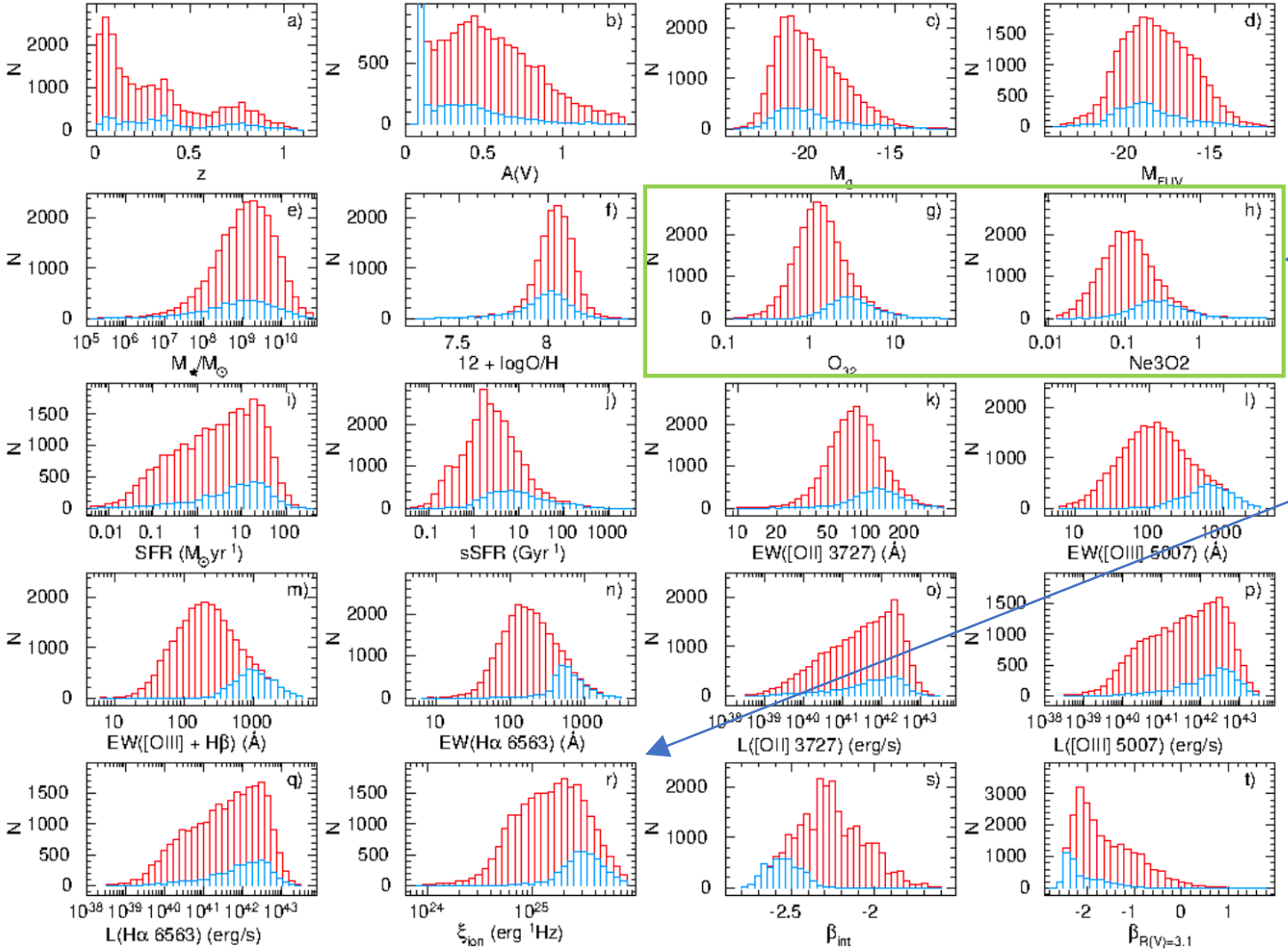

Fig. 2. Histograms of the **(a)** redshift z, **(b)** extinction $A(V)$ in the V band derived from the hydrogen Balmer decrement, **(c)** absolute g-band magnitude M_g corrected for the Milky Way extinction, **(d)** 'observed' absolute FUV magnitude $M_{\rm FUV}$, i.e. the absolute magnitude derived from the extrapolation of the extinction-corrected SDSS spectrum and attenuated adopting extinction $A(V)$ obtained from the Balmer hydrogen decrement, **(e)** stellar mass derived from the SED fitting of the extinction-corrected SDSS spectrum, **(f)** oxygen abundance 12 + logO/H, **(g)** [O III] λ5007/[O II] λ3727 ratio denoted as O_{32}, **(h)** [Ne III] λ3868/[O II] λ3727 ratio denoted as Ne3O2, **(i)** star-formation rate SFR derived from the extinction-corrected Hβ luminosity, **(j)** specific star-formation rate sSFR = SFR/($M_\star$/M$_\odot$), **(k) - (n)** equivalent widths of the [O II] λ3727, [O III] λ5007, Hβ + [O III] λ4959 + [O III] λ5007 and Hα emission lines, respectively, **(o) - (q)** extinction-corrected luminosities of the [O II] λ3727, [O III] λ5007 and Hα λ6563 emission lines, respectively, **(r)** ionising photon production efficiency derived from the extinction-corrected Hβ luminosity and extinction-corrected monochromatic luminosity at the rest-frame wavelength of 1500Å, **(s)** extinction-corrected UV slope derived from the modelled rest-frame SED, **(t)** UV slope derived from the obscured SEDs with the extinction coefficient derived from the observed Balmer decrement adopting the Cardelli et al. (1989) reddening law with $R(V) = 3.1$. In all panels, histograms represented by the red and blue lines are for the total SDSS sample of CSFGs and for CSFGs with EW(Hβ) $\geq$ 100Å, respectively.

Зависят от ионизационного параметра (-> более молодой возраст вспышек ЗО при EW(Hbeta)>100A)

$$\xi_{\rm ion} = \frac{N({\rm LyC})}{L_\nu}$$

Эффективность производства ионизующих квантов (выше в галактиках с более высокой EW(Hβ)).
В случае EW(Hβ)>100A согласуется с тем, что нужно для реионизации на больших z.

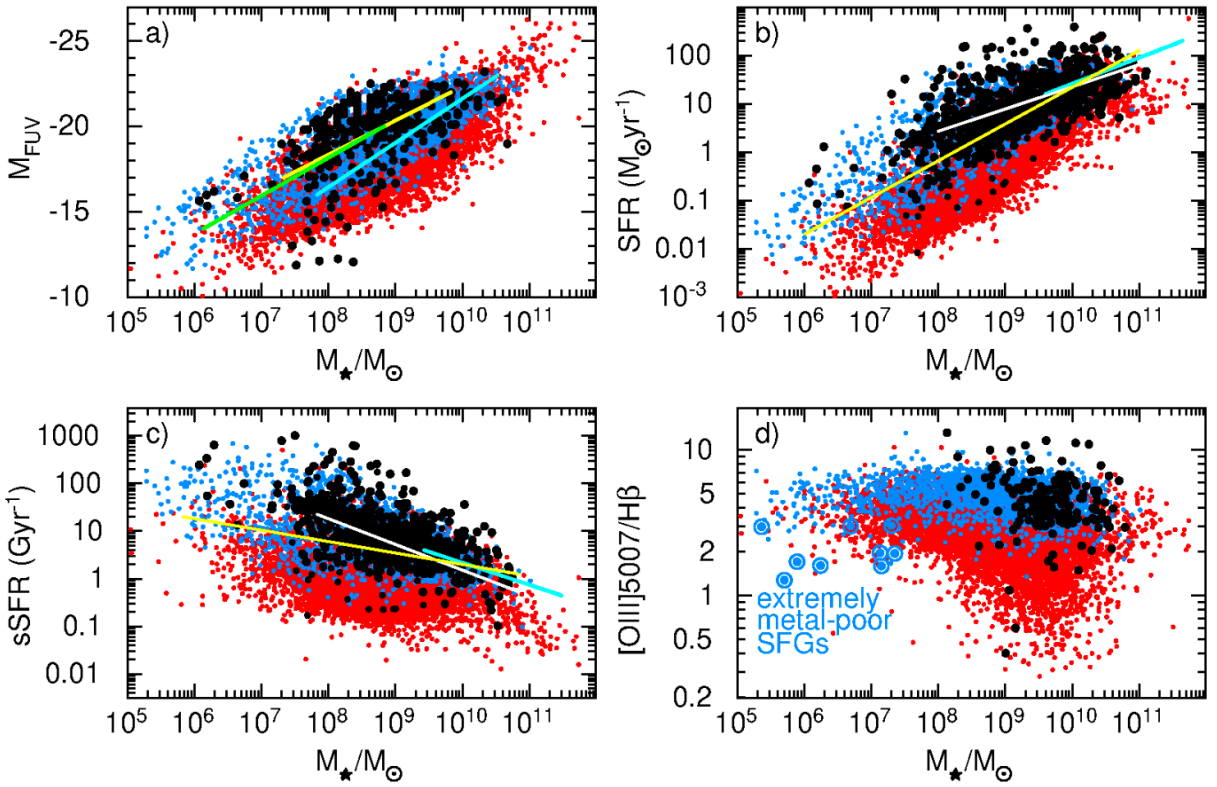

Fig. 3. **(a)** Dependence of the FUV absolute magnitude on the stellar mass $M_\star$. Black-filled circles are high-z galaxies (Bridge et al. 2019; Endsley et al. 2021; Karman et al. 2017; Rasappu et al. 2016; Khusanova et al. 2020; Tang et al. 2020; Strait et al. 2020b; Santos et al. 2020). Relations for high-z galaxies by Song et al. (2016), Grazian et al. (2015) and Yung et al. (2019) are represented by yellow, cyan and green lines, respectively. **(b), (c)** SFR versus the stellar mass and the sSFR versus the stellar mass, respectively. Black-filled circles in both panels are high-z galaxies (Karman et al. 2017; Amorín et al. 2016; Sanders et al. 2020a; Erb et al. 2016; Holden et al. 2016; Khusanova et al. 2020; Rasappu et al. 2016; Santos et al. 2020; Troncoso et al. 2014; Strait et al. 2020a; Reddy et al. 2006; Hagen et al. 2016; Onodera et al. 2016; Santini et al. 2017; Cullen et al. 2014; Saxena et al. 2020; Endsley et al. 2021, 2020; Tang et al. 2020; Strait et al. 2020b; Jones et al. 2020). White solid lines, yellow solid lines and cyan solid lines in **(b)** and **(c)** represent relations for high-z galaxies by Arrabal Haro et al. (2020), Iyer et al. (2018) and Florez et al. (2020), respectively. **(d)** The dependence of the [O III] λ5007/Hβ flux ratio on the stellar mass $M_\star$. Black filled citcles represent high-z galaxies (Richard et al. 2011; Schenker et al. 2013; Steidel et al. 2014; Troncoso et al. 2014; Holden et al. 2016). The most metal-poor nearby galaxies with 12 + log O/H ~ 6.9 – 7.25 (Izotov et al. 2018c; Kojima et al. 2020, Izotov et al., in preparation) are shown by encircled blue-filled circles. The meanings of other symbols in all panels are the same as in Fig. 1.

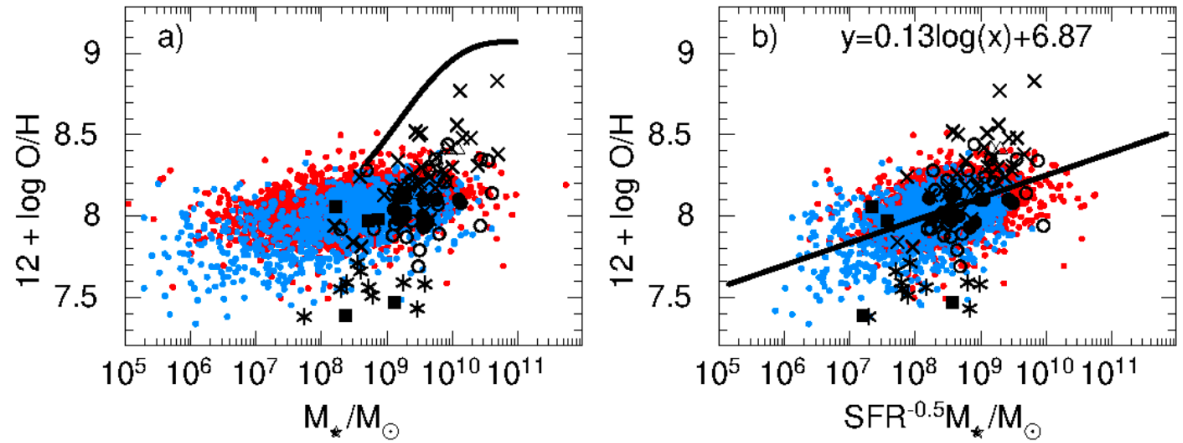

Fig. 4. Dependences of oxygen abundances 12 + logO/H on **(a)** stellar masses $M_\star$ and on **(b)** $SFR^{-0.5}M_\star$ for the samples of CSFGs and high-z SFGs. The maximum likelihood relation to SDSS data in **(b)** is shown by the straight solid line. The black line in **(a)** is the relation for $z = 0$ SDSS SFGs by Mannucci et al. (2010). Large symbols represent high-z SFGs by Amorín et al. (2016) (z = 2.4–3.5, asterisks), Erb et al. (2016) (z ~ 2.3, filled circles), Troncoso et al. (2014) (z ~ 3–5, open circles), Onodera et al. (2016) (z ~ 3 – 3.7, crosses), Cullen et al. (2014) ($z > 2$, open triangles) and Jones et al. (2020) (z = 7.1 – 9.1, filled squares). The meanings of symbols for SDSS CSFGs in both panels are the same as in Fig. 1.

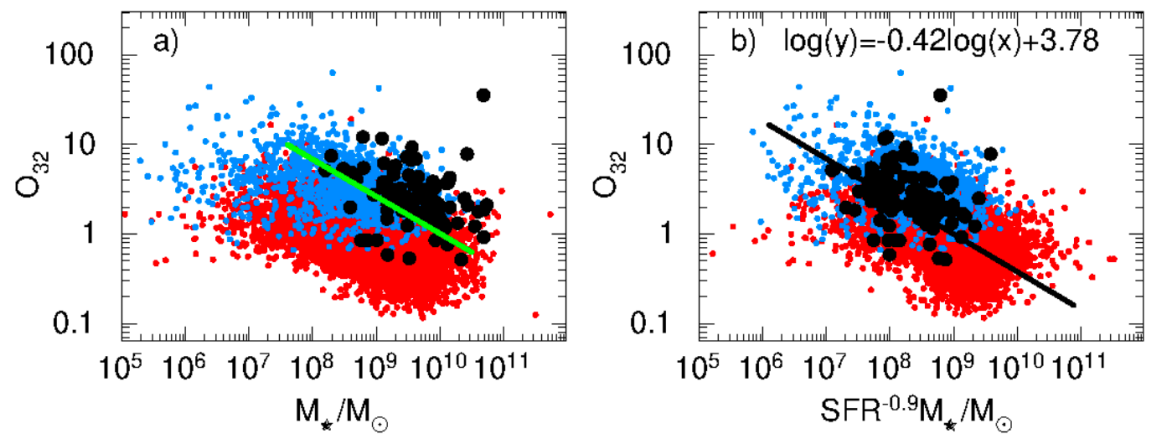

Fig. 5. Dependences of O_{32} = [O III] λ5007/[O II] λ3727 emission line ratios on **(a)** stellar masses $M_\star$ and on **(b)** $SFR^{-0.9}M_\star$ for samples of CSFGs and high-z SFGs. The black line in **(b)** is the maximum likelihood relation whereas the green line in **(a)** is the relation for z ~ 1.7 – 3.6 galaxies (Sanders et al. 2020a). Black-filled circles represent high-z SFGs by Erb et al. (2016) (z ~ 2.3), Onodera et al. (2016) (z ~ 3 – 3.7), Troncoso et al. (2014) (z ~ 3 – 5), and Cullen et al. (2014) (stacks of $z > 2$ galaxies). The meaning of symbols for our SDSS are the same as in Fig. 1.

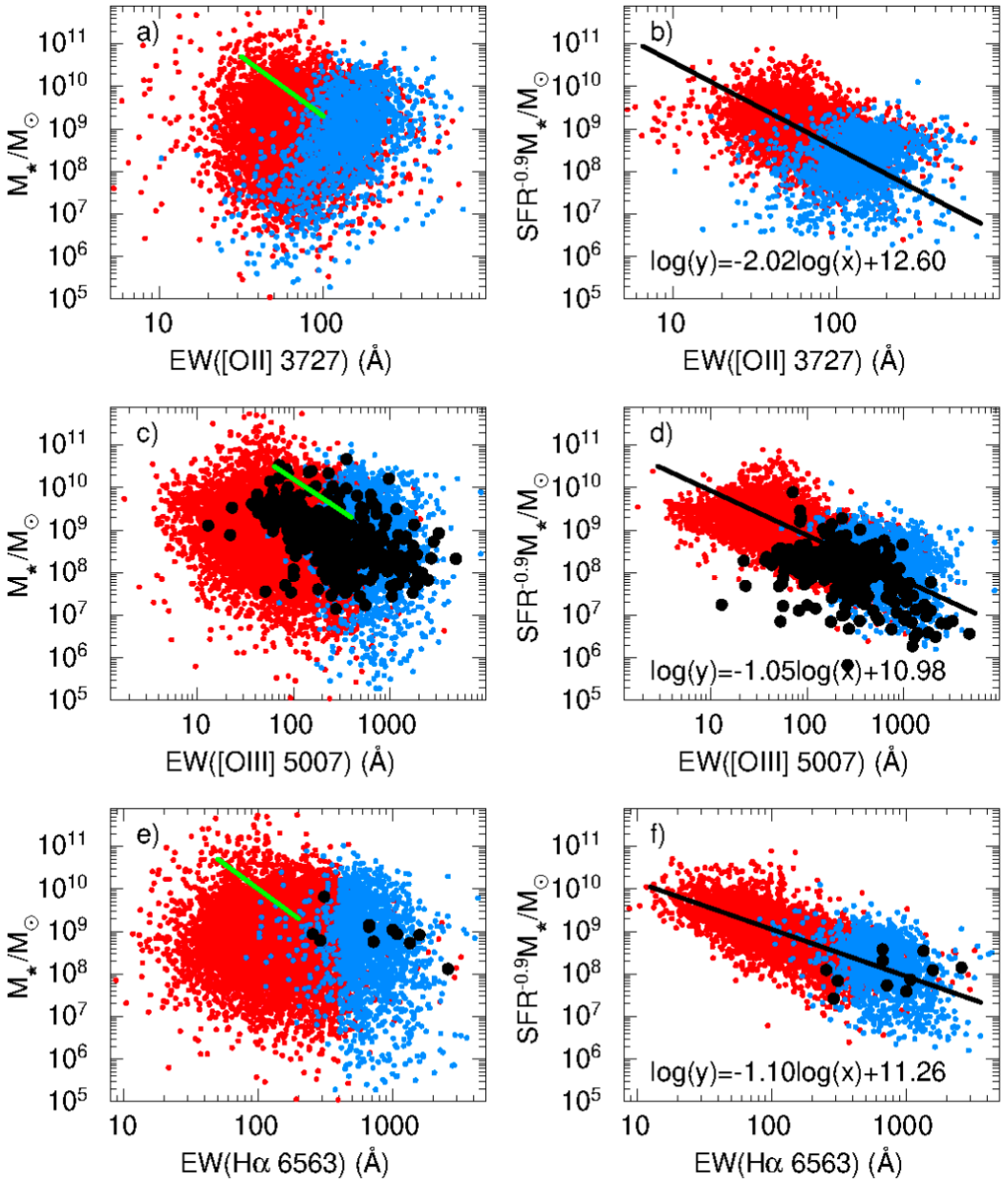

Fig. 6. Dependences of stellar masses $M_\star$ (**(a)**, **(c)**, **(e)**) and of $SFR^{-0.9}M_\star$ (**(b)**, **(d)**, **(f)**) on the equivalent widths of the [O II] λ3727, [O III] λ5007 and Hα λ6563 emission lines, respectively, for samples of CSFGs and high-z SFGs. The solid lines in **(b)**, **(d)**, **(f)** are the maximum likelihood relations, whereas green lines in **(a)**, **(c)**, **(e)** are relations for $z \sim 1.4 - 3.8$ SFGs (Reddy et al. 2018). Galaxies denoted in **(c)** and **(d)** by black-filled circles are $z \sim 3.5$ LBGs (Holden et al. 2016), $z \sim 2$ SFGs (Hagen et al. 2016), $z \sim 1.3 - 3.7$ galaxies with high EW([O III] + Hβ) (Tang et al. 2020), $z \sim 7$ SFGs with high EW([O III] + Hβ) (Endsley et al. 2021), $z \sim 6.6$ SFGs with Lyα emission (Endsley et al. 2020) and $z \sim 8$ galaxies (De Barros et al. 2019). Galaxies represented in **(e)** and **(f)** by black-filled circles are $z \sim 5$ SFGs by Rasappu et al. (2016). The meanings of symbols for our SDSS CSFGs are the same as in Fig. 1.

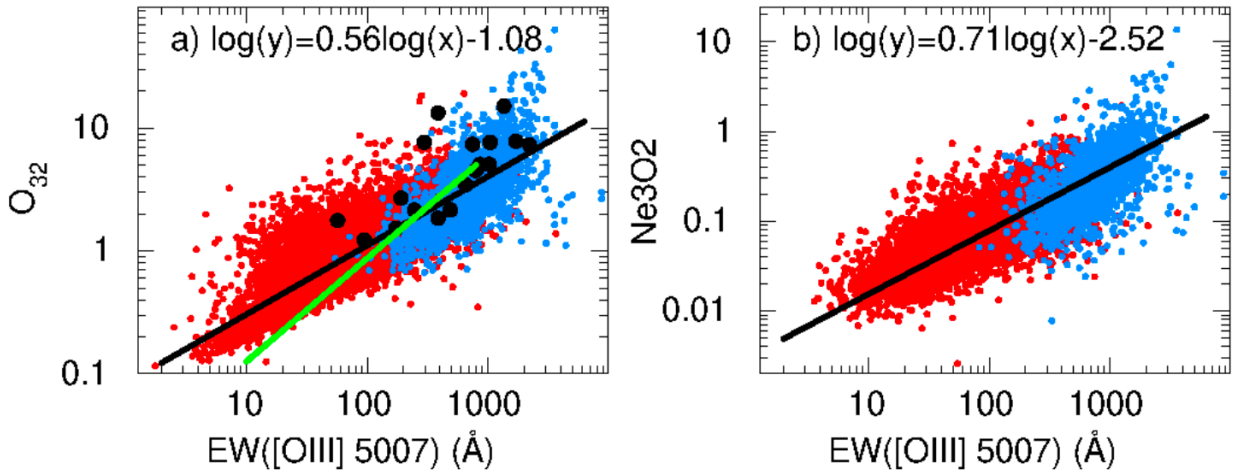

Fig. 7. Relations between equivalent widths of the [O III] λ5007 emission line and extinction-corrected **(a)** O_{32} = [O III] λ5007/[O II] λ3727 and **(b)** Ne3O2 = [Ne III] λ3868/[O II] λ3727 for samples of CSFGs and high-z SFGs. The solid lines are the maximum likelihood relations, whereas the green line in **(a)** is the relation for $z \sim 1.4 - 3.8$ galaxies (Reddy et al. 2018). LAEs at $z \sim 3$ by Nakajima et al. (2020) are shown in **(a)** by filled black circles. The meanings of symbols for SDSS CSFGs are the same as in Fig. 1.

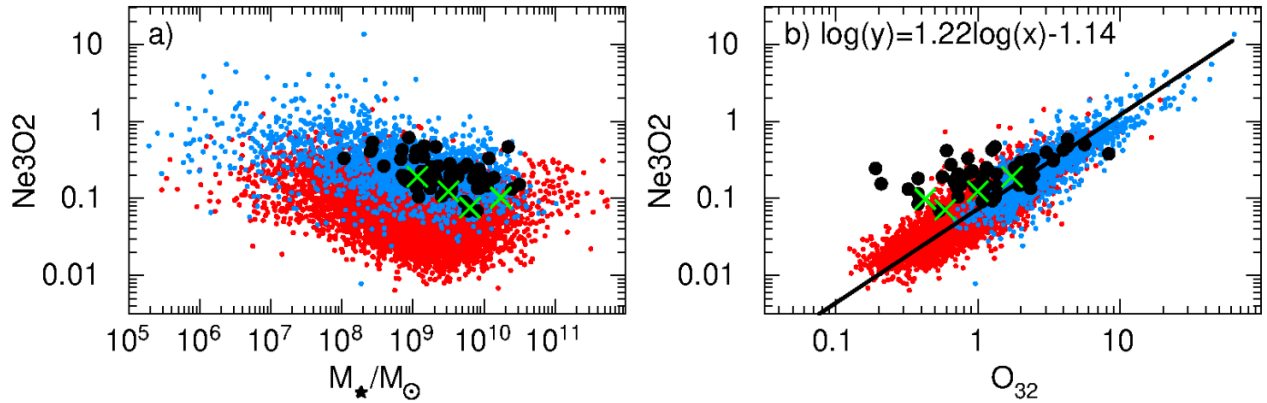

Fig. 8. Dependences of Ne3O2 = [Ne III] λ3868/[O II] λ3727 on **(a)** stellar masses $M_\star$ and **(b)** the O_{32} = [O III] λ5007/[O II] λ3727. The solid line in **(b)** is the maximum likelihood relation. The individual $z \sim 2$ SFGs from the MOSDEF survey and stacks of MOSDEF spectra from Jeong et al. (2020) are shown by black-filled circles and green crosses, respectively. The meanings of symbols for CSFGs are the same as in Fig. 1.

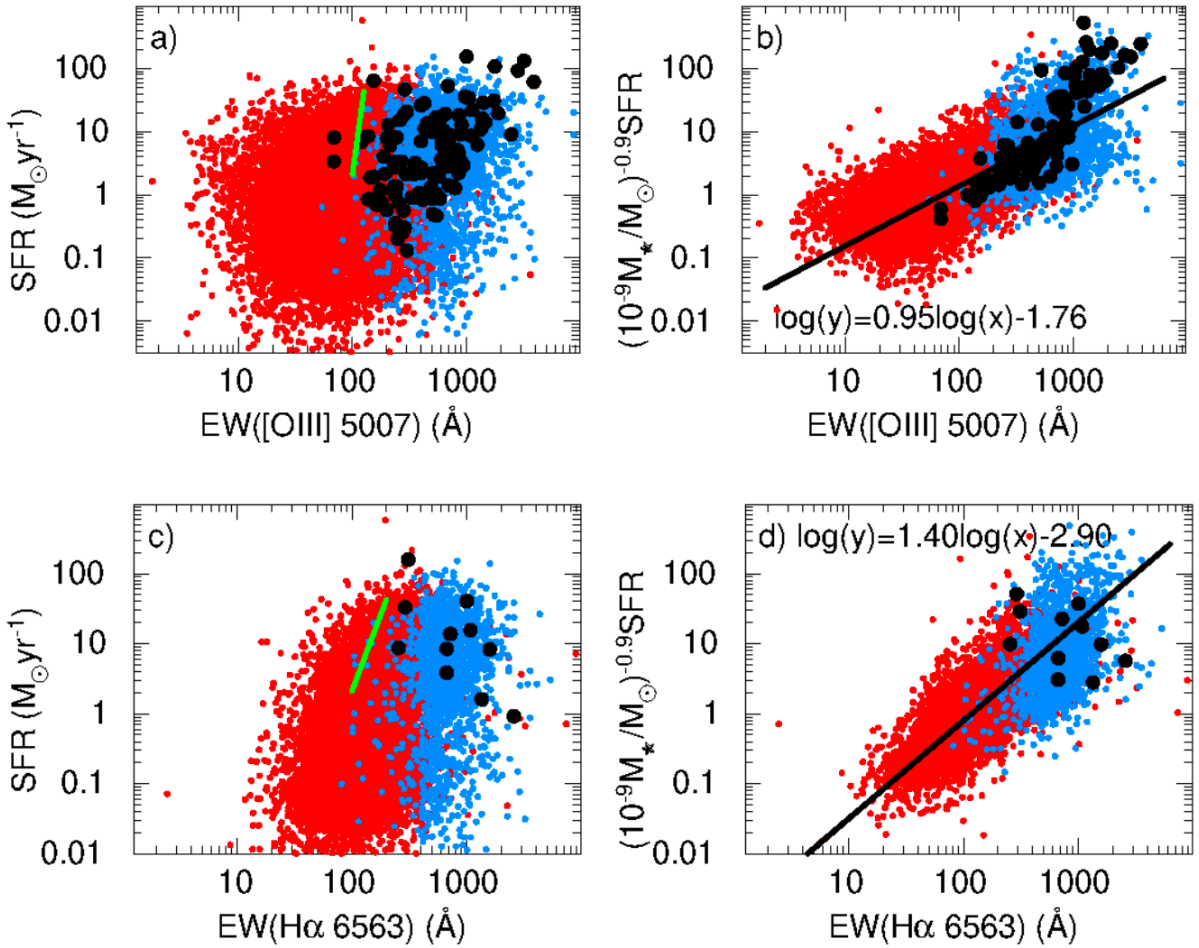

Fig. 9. Dependences of star-formation rates SFR ((**a**), (**c**)) and of $M_\star^{-0.9}$SFR ((**b**), (**d**)) on equivalent widths of the [O III] λ5007 and H emission lines, respectively, for samples of CSFGs and high-z SFGs. The solid lines in (**b**) and (**d**) are the maximum likelihood relations. denoted in (**a**) and (**b**) by black-filled circles are $z \sim 3.5$ LBGs by Holden et al. (2016), $z \sim 1.3 - 3.7$ galaxies with high EW([O III] + Hβ) et al. (2020), $z \sim 7$ galaxies with high EW([O III] + Hβ) by Endsley et al. (2021) and $z \sim 6.6$ galaxies with Lyα emission by Endsley et al respectively. Galaxies represented in (**c**) and (**d**) by black-filled circles are $z \sim 5$ SFGs by Rasappu et al. (2016). Green lines in (**a**) and (**c** relations for $z = 1.4 - 3.8$ SFGs (Reddy et al. 2018). The meanings of symbols for SDSS CSFGs are the same as in Fig. 1.

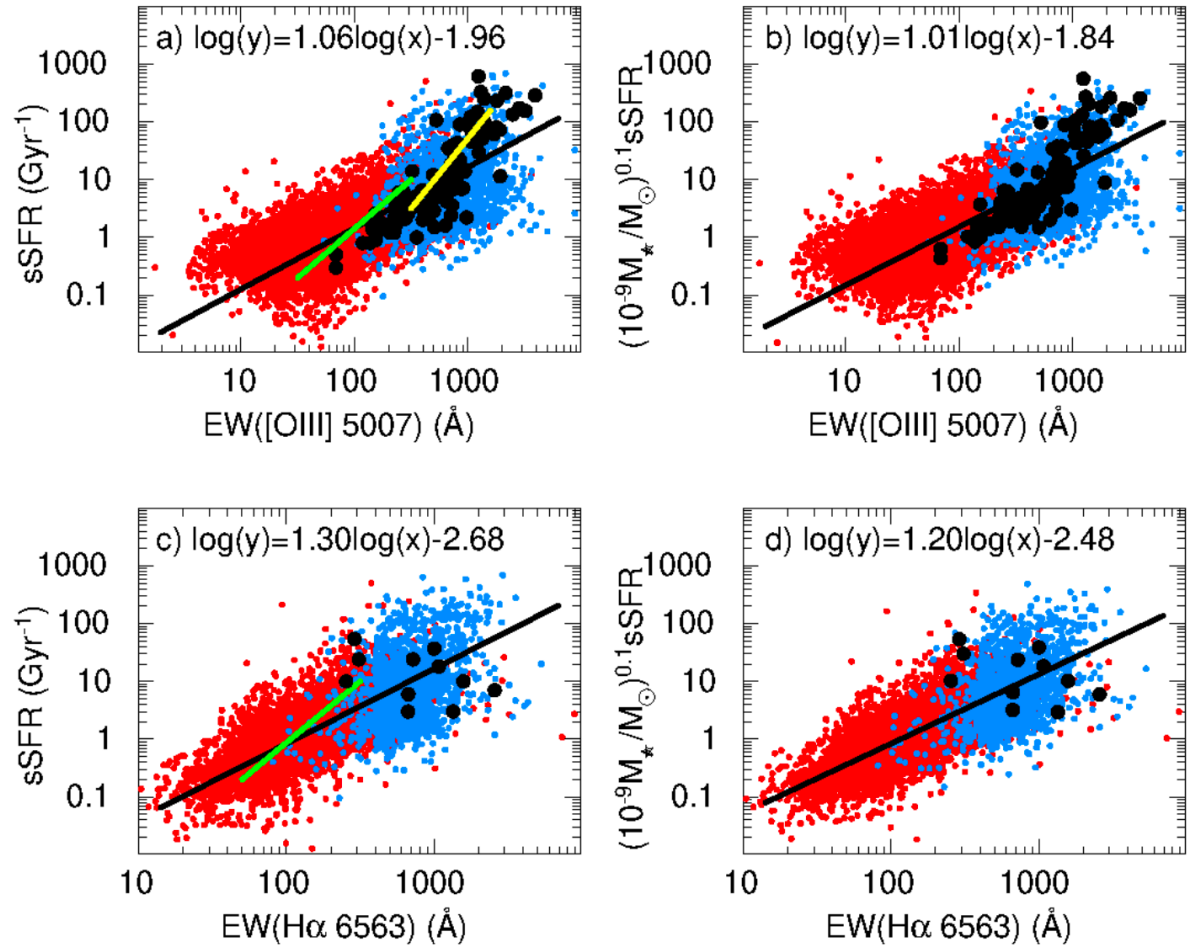

Fig. 10. Dependences of specific star-formation rates sSFR ((**a**), (**c**)) and of $M_\star^{-0.1}$sSFR ((**b**), (**d**)) on equivalent widths of the [O III] λ5007 and Hα λ6563 emission lines, respectively, for samples of CSFGs and high-z SFGs. Solid lines are the maximum likelihood relations. Galaxies denoted in (**a**) and (**b**) by black-filled circles are $z \sim 3.5$ LBGs by Holden et al. (2016), $z \sim 1.3 - 3.7$ galaxies with high EW([O III] + Hβ) by Tang et al. (2020), $z \sim 7$ galaxies with high EW([O III] + Hβ) by Endsley et al. (2021) and $z \sim 6.6$ galaxies with Lyα emission by Endsley et al. (2020). Galaxies represented in (**c**) and (**d**) by black-filled circles are $z \sim 5$ SFRs by Rasappu et al. (2016). Yellow and green solid lines in (**a**) represent relations of $z \sim 2$ analogues for $z > 6.5$ galaxies (Du et al. 2020) and $z = 1.4 - 3.8$ SFGs (Reddy et al. 2018), respectively, whereas the relation for $z = 1.4 - 3.8$ SFGs (Reddy et al. 2018) in (**c**) is shown by the green line. The meanings of symbols for SDSS CSFGs are the same as in Fig. 1.

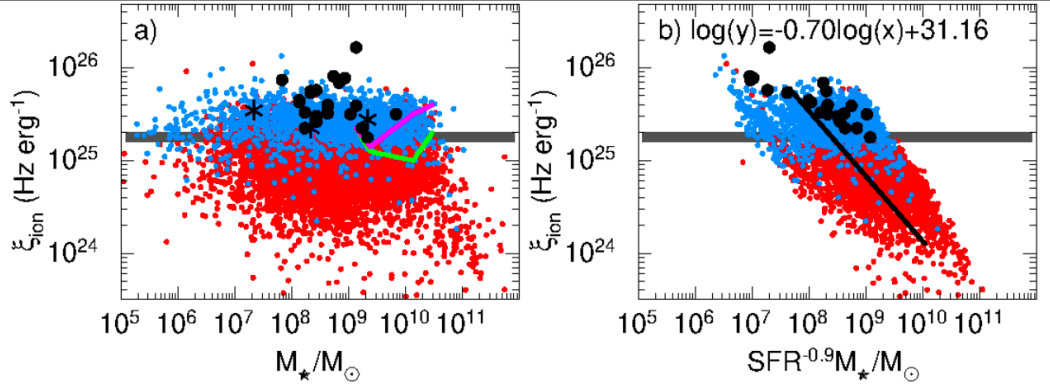

Fig. 11. Relations between ionising photon production efficiences ξ_{ion} and stellar masses $M_\star$ **(a)** and $SFR^{-0.9}M_\star$ **(b)** for samples of CSFGs and high-z SFGs. The solid line in **(b)** is the maximum likelihood relation whereas stacks for $z \sim 1.4 - 2.6$ SFGs (Shivaei et al. 2018) for Calzetti et al. (1994, 2000) and SMC reddening laws are shown in **(a)** by green and magenta lines, respectively. Mean ξ_{ion} values of $z = 4 - 5$ galaxies (Lam et al. 2019a) in the three stellar mass bins are shown in **(a)** by asterisks, whereas $z \sim 6.6$ SFGs with Lyα emission by Endsley et al. (2020) are represented in both panels by filled circles. Values of ξ_{ion} assumed in canonical Universe reionisation models are shown with a thick horizontal grey line (e.g. Bouwens et al. 2016). The meanings of symbols for the SDSS CSFGs are the same as in Fig. 1.

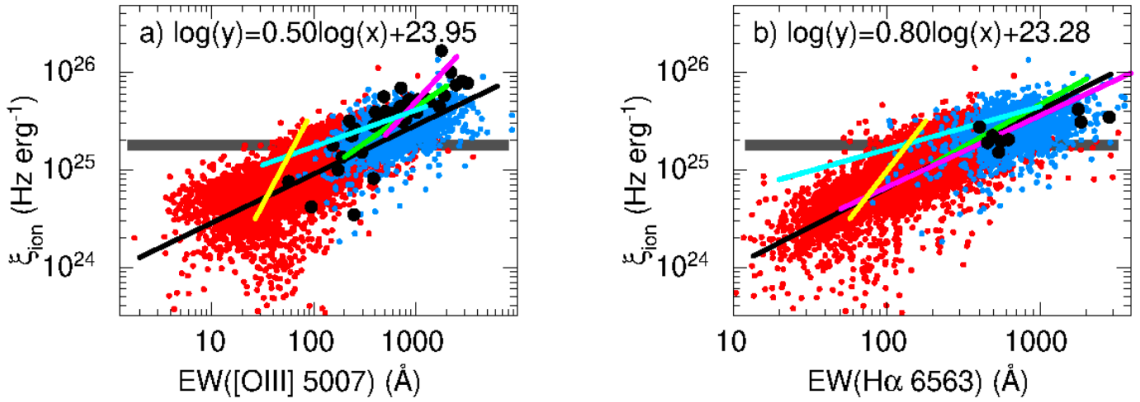

Fig. 12. **(a)** and **(b)** Relations between ionising photon production efficiences, ξ_{ion}, and equivalent widths of the [O III] λ5007 and Hα λ6563 emission lines for samples of CSFGs and high-z SFGs. The black solid lines are the maximum likelihood relations whereas green, magenta, cyan, and yellow solid lines in **(a)** are the relations for $z \sim 1.3 - 2.7$ strong [O III] emitters (Tang et al. 2019), $z \sim 0$ SFGs with EW([O III]) > 1000Å (Chevallard et al. 2018), $z \sim 2$ lensed galaxies (Emami et al. 2020), and $z \sim 1.4 - 3.8$ galaxies (Reddy et al. 2018), respectively; LAEs at $z \sim 3$ (Nakajima et al. 2020) and $z \sim 6.6$ SFGs with Lyα emission (Endsley et al. 2020) are shown in **(a)** by filled black circles. Mean ξ_{ion} values for $z = 4 - 5$ galaxies (Lam et al. 2019a) are shown in **(b)** by filled circles. The lines in **(b)** are the relations for $z \sim 1.3 - 2.7$ strong [O III] emitters (green line, Tang et al. 2019), $z \sim 4 - 6$ SFGs (magenta line, Faisst et al. 2019), $z \sim 2$ lensed galaxies (cyan line, Emami et al. 2020), and $z \sim 1.4 - 3.8$ (yellow line, Reddy et al. 2018). Values for ξ_{ion} assumed in canonical Universe reionisation models are shown with a thick horizontal grey line (e.g. Bouwens et al. 2016). The meanings of symbols for SDSS CSFGs are the same as in Fig. 1.

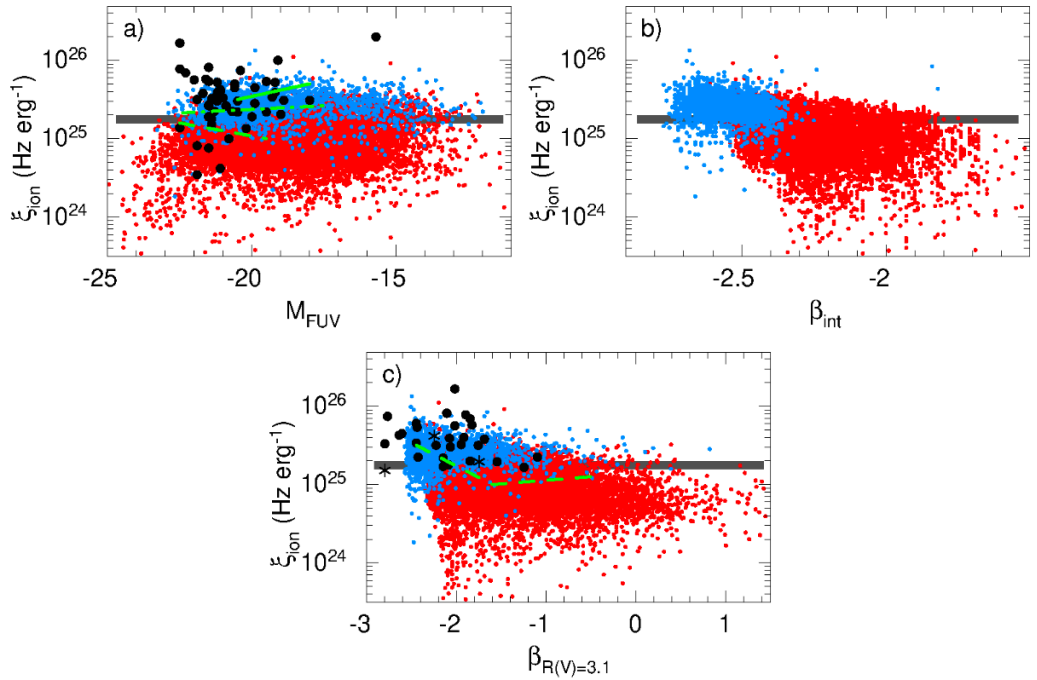

Fig. 13. **(a)** Dependence of the ionising photon production efficiency ξ_{ion} on the UV absolute magnitude M_{FUV}. The LAEs at $z \sim 3$ (Nakajima et al. 2020), $z \sim 6.6$ SFGs with Lyα emission (Endsley et al. 2020), mean ξ_{ion} values for $z = 3.8 - 5.4$ galaxies (Bouwens et al. 2016), mean ξ_{ion} values for $z = 4 - 5$ galaxies (Lam et al. 2019a), and a mean ξ_{ion} value for $z = 3.8 - 5.4$ faint galaxies with high EW(Lyα) (Maseda et al. 2020) are shown by filled circles. The relation for ~ 2 galaxies (Shivaei et al. 2018), for $z \sim 9 - 10$ galaxies (Bouwens et al. 2019) and for $z \sim 3$ faint Lyα emitters (Nakajima et al. 2018) are shown by a green dashed, dash-dotted and solid lines, respectively. **(b)** Dependence of the ionising photon production efficiency ξ_{ion} on the intrinsic UV slope β. **(c)** Dependence of the ionising photon production efficiency ξ_{ion} on the intrinsic UV slope β reddened with $R(V) = 3.1$. Filled circles are $z \sim 3.8 - 5.4$ galaxies (Bouwens et al. 2016) and $z \sim 6.6$ SFGs with Lyα emission (Endsley et al. 2020), asterisks are mean ξ_{ion} values of $z = 4 - 5$ galaxies (Lam et al. 2019a). The relation for $z \sim 2$ galaxies (Shivaei et al. 2018) is shown by a green dashed line. Values of ξ_{ion} assumed in canonical Universe reionisation models are shown (as in Figs. 11 and 12 in grey (e.g. Bouwens et al. 2016). The meanings of symbols for the SDSS CSFGs are the same as in Fig. 1.

Вывод:

Близкие CSFGs очень похожи по всем известным свойствам на галактики z ~ 1.5 – 10.

Не обнаружено никаких отличий между этими типами объектов, что делает CSFGs хорошими аналогами галактик на больших z.

J2229+2725: an extremely low-metallicity dwarf compact star-forming galaxy with an exceptionally high [O III]λ5007/[O II]λ3727 flux ratio of 53

Y. I. Izotov[1⋆], T. X. Thuan[2] and N. G. Guseva[1]
[1] *Bogolyubov Institute for Theoretical Physics, National Academy of Sciences of Ukraine, 14-b Metrolohichna str., Kyiv, 03143, Ukraine,*
[2] *Astronomy Department, University of Virginia, P.O. Box 400325, Charlottesville, VA 22904-4325,*

19 April 2021

ABSTRACT

Using the Large Binocular Telescope (LBT)/Multi-Object Dual Spectrograph (MODS), we have obtained optical spectroscopy of one of the most metal-poor dwarf star-forming galaxies (SFG) in the local Universe, J2229+2725,. This galaxy with a redshift z=0.0762 was selected from the Data Release 16 (DR16) of the Sloan Digital Sky Survey (SDSS). Its properties derived from the LBT observations are most extreme among SFGs in several ways. Its oxygen abundance 12 + logO/H = 7.085±0.031 is among the lowest ever observed for a SFG. With its very low metallicity, an absolute magnitude $M_g = -16.39$ mag, a low stellar mass $M_\star = 9.1\times10^6$ $M_\odot$ and a very low mass-to-light ratio $M_\star/L_g \sim 0.0166$ (in solar units), J2229+2725 deviates strongly from the luminosity-metallicity relation defined by the bulk of the SFGs in the SDSS. J2229+2725 has a very high specific star-formation rate sSFR ~ 75 Gyr^{-1}, indicating very active ongoing star formation. Three other features of J2229+2725 are most striking, being the most extreme among lowest-metallicity SFGs: 1) a ratio $O_{32} = I([\text{O III}]\lambda5007)/I([\text{O II}]\lambda3727) \sim 53$, 2) an equivalent width of the Hβ emission line EW(Hβ) of 577Å, and 3) an electron number density of ~ 1000 cm^{-3}. These properties imply that the starburst in J2229+2725 is very young. Using the extremely high O_{32} in J2229+2725, we have improved the strong-line calibration for the determination of oxygen abundances in the most metal-deficient galaxies, in the range 12 + logO/H $\lesssim$ 7.3.

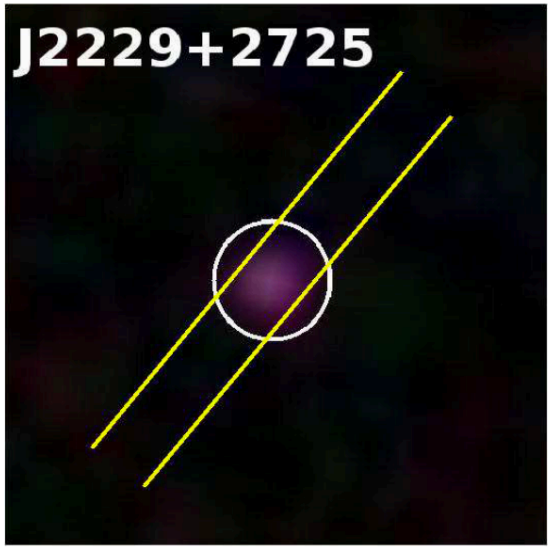

Figure 1. 12 arcsec × 12 arcsec region with the color composite SDSS image of J2229+2725. The 2 arcsec SDSS spectroscopic aperture and 1.2 arcsec wide LBT/MODS slit are indicated by a white circle and yellow parallel lines, respectively.

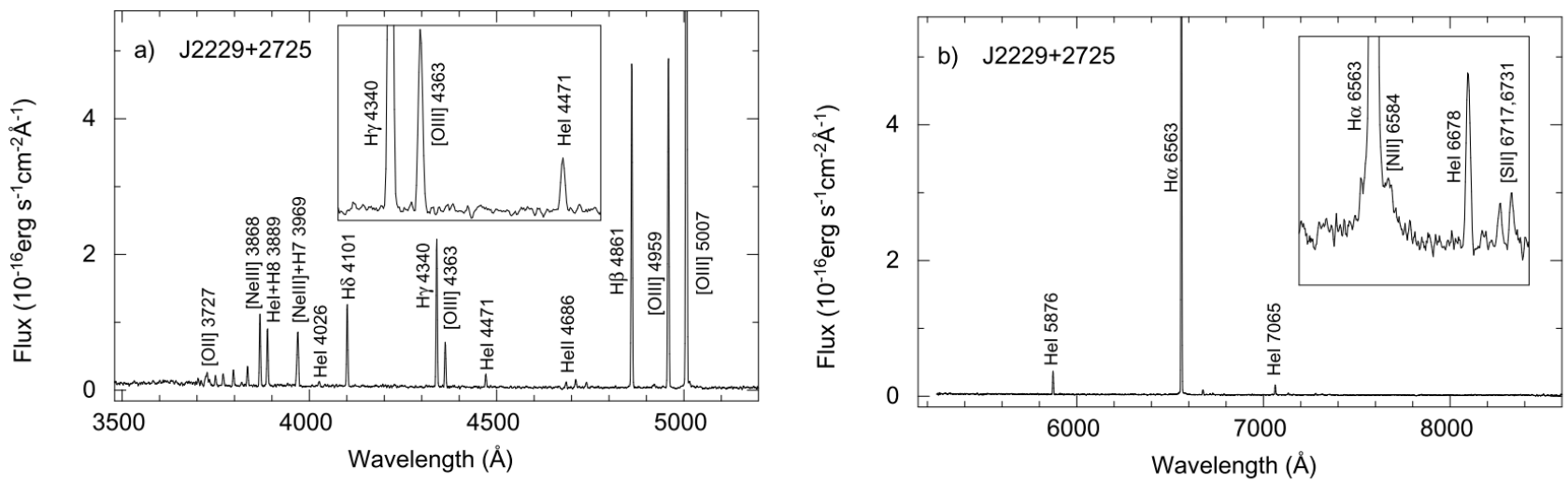

Figure 2. The rest-frame LBT spectrum of J2229+2725. Insets in **a)** and **b)** show expanded parts of the spectral regions around the Hγ and Hα emission lines, respectively, for a better view of weak features. Some emission lines are labelled.

Table 1. Observed and derived characteristics of J2229+2725

Parameter	J2229+2725
R.A.(J2000)	22:29:33.19
Dec.(J2000)	+27:25:25.60
z	0.07622
GALEX FUV, mag	21.45±0.28
GALEX NUV, mag	21.88±0.37
SDSS u, mag	21.96±0.15
SDSS g, mag	21.47±0.04
SDSS r, mag	22.27±0.11
SDSS i, mag	20.97±0.05
SDSS z, mag	21.43±0.33
D_L, Mpc*	347
M_g, mag†	−16.39±0.06
log $L_g/\mathrm{L}_{g,\odot}$‡	8.74
log $M_\star/\mathrm{M}_\odot$††	6.96
$M_\star/L_g$, $\mathrm{M}_\odot/\mathrm{L}_{g,\odot}$	0.0166
$L(\mathrm{H}\beta)$, erg s^{-1}**	$(3.1\pm0.3)\times10^{40}$
SFR, $\mathrm{M}_\odot\mathrm{yr}^{-1}$‡‡	0.68±0.06
sSFR, Gyr^{-1}	75
12+logO/H†††	7.085±0.031

*Luminosity distance.
†Absolute magnitude corrected for Milky Way extinction.
‡log of the SDSS g-band luminosity corrected for Milky Way extinction.
††Stellar mass derived from the extinction-corrected SDSS spectrum.
**Hβ luminosity derived from the extinction-corrected SDSS spectrum.
‡‡Star formation rate derived from the Kennicutt (1998) relation using the extinction-corrected Hβ luminosity.
†††Oxygen abundance derived from the LBT spectrum.

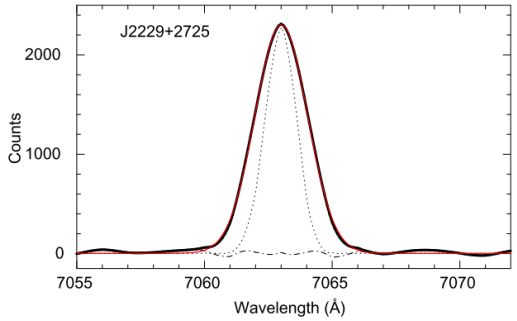

Figure 3. The Hα profile in the medium-resolution DIS spectrum of J2229+2725. The observed spectrum is shown by a black solid line while the Gaussian fit is represented by a red solid line. The black dash-dotted line shows the residual spectrum after subtraction of the Hα fit. The instrumental profile is represented by a black dotted line.

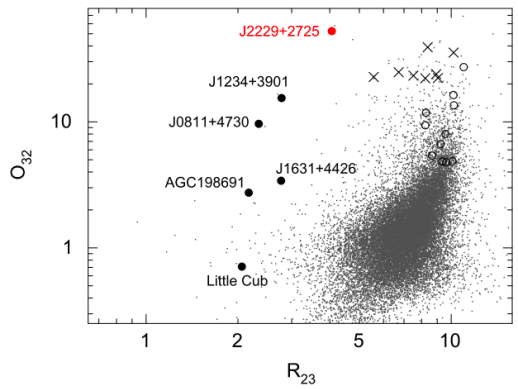

Figure 4. The O_{32} – R_{23} diagram for compact SFGs, where O_{32}= I([O III]λ5007)/I([O II]λ3727) and R_{23} = I([O II]λ3727 + [O III]λ4959 + [O III]λ5007)/I(Hβ). The lowest-metallicity SFGs known with 12 + log O/H < 7.1 from Hirschauer et al. (2016, A198691), Hsyu et al. (2017, Little Cub), Izotov et al. (2018a, J0811+4730), Izotov et al. (2019a, J1234+3901), Kojima et al. (2020, J1631+4426) and this paper (J2229+2725) are shown by labelled filled circles. LyC leakers from Izotov et al. (2016a,b, 2018b,c) are shown by open circles. SFGs with the highest O_{32} from Izotov et al. (2020) are represented by crosses and compact SFGs from the SDSS DR16 by grey dots.

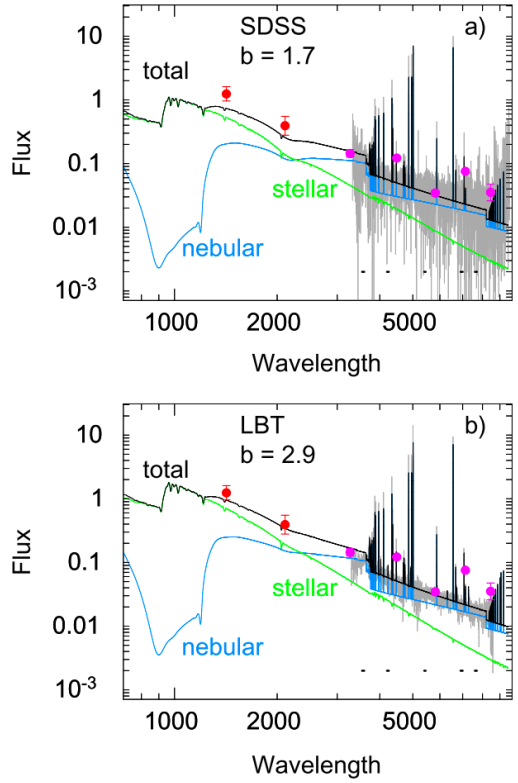

Figure 5. a) and **b)** Best-fit spectral energy distributions obtained from fitting the rest-frame SDSS and LBT spectra, respectively, by randomly varying t_b, t_1, t_2 and $b = M_{old}/M_{young}$, where t_b is the age of young stellar population, $t_2 - t_1$ is the interval, in which the old stellar population was formed. In both panels, the observed spectra are shown in grey, the modelled stellar, nebular and total SEDs are shown by green, blue and black lines, respectively, and are labelled. *GALEX* FUV, NUV and SDSS u, g, r, i and z photometric data, blueshifted adopting the J2229+2725 redshift, are shown by red and magenta filled circles, respectively. Short horizontal lines represent intervals used for continuum fitting, which are free of emission lines. Fluxes are in units 10^{-16} erg s^{-1}cm^{-2}Å^{-1} and wavelengths are in Å.

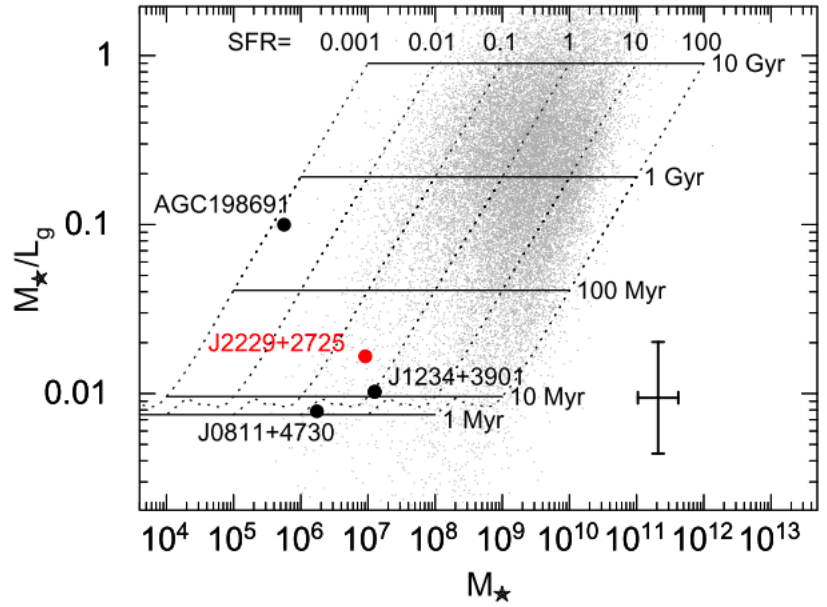

Figure 6. Relation between the stellar mass-to-luminosity ratio and the stellar mass of SFGs. All quantities are expressed in solar units. Selected lowest-metallicity SFGs J0811+4730, J1234+3901 and AGC 198691 with 12+logO/H $\sim$ 7.0 are represented by labelled black filled circles. The galaxy J2229+2725 is shown by a red filled circle. The error bars indicate the errors of $M_\star$ and $M_\star/L_g$ for that SFG. For comparison, compact SFGs from the SDSS DR16 with redshifts $z > 0.01$ (grey dots) are also shown. Dotted lines represent Starburst99 models with continuous star formation and a SFR varying from 0.001 to 100 M$_\odot$ yr^{-1}, during periods from the present to 10 Gyr, 1 Gyr, 100 Myr, 10 Myr, and 1 Myr in the past (horizontal solid lines). These models include the contribution of both the stellar and nebular continua.

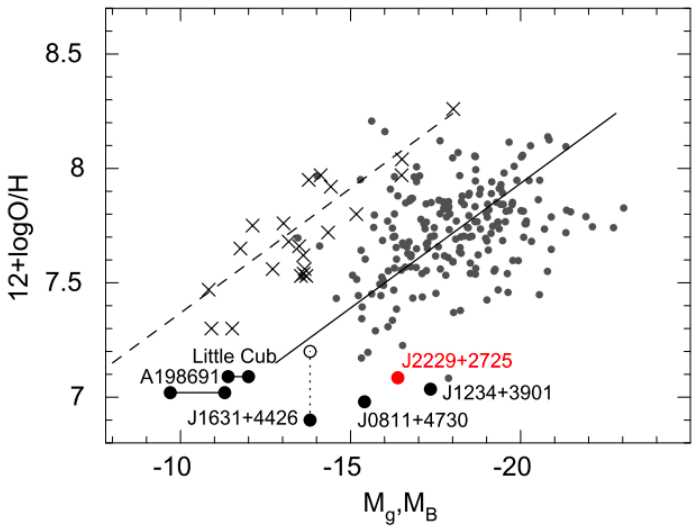

Figure 7. The oxygen abundance - absolute magnitude diagram. The most metal-poor galaxies (the same ones as in Fig. 4) are represented by filled and open circles. Low-luminosity galaxies are represented by crosses, with the fit to these data by Berg et al. (2012) shown by a dashed line. The solid line is the fit to the SDSS compact SFGs from DR16 with EW(Hβ) $\geqslant$ 200Å and oxygen abundances derived by the direct T_e method (grey dots). This subsample of SDSS galaxies includes only compact galaxies with [O III]λ4363 emission lines in their spectra, measured with errors less than 20 per cent of their fluxes. The vertical dotted line for J1631+4426 connects the locations of the galaxy with oxygen abundances derived by the direct T_e method (filled circle) and by the strong-line method (open circle, see Sect. 7). The horizontal lines connect the positions of the nearby galaxies AGC 198691 and Little Cub, calculated with two different distances.

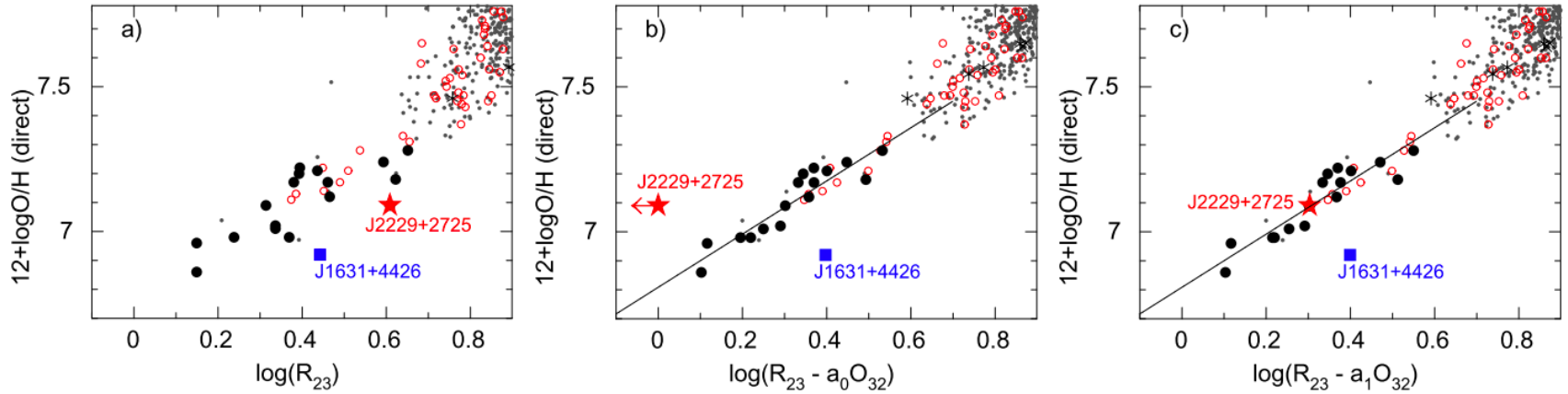

Figure 8. The **a)** (log R_{23}) - (12 + logO/H), **b)** log(R_{23} - a_0O_{32}) - (12 + logO/H), and **c)** log(R_{23} - a_1O_{32}) - (12 + logO/H) relations, where $a_0 = 0.080$ (Izotov et al. 2019b) and $a_1 = 0.080 - 0.00078O_{32}$ (this paper). In all these relations 12 + logO/H is derived by the direct method, R_{23} = ([O III]λ4959+λ5007 + [O II]λ3727)/Hβ and O_{32} = [O III]λ5007/[O II]λ3727. The galaxy J2229+2725 is shown by a red filled star, while J1631+4426 (Kojima et al. 2020) is represented by a blue filled square. Other lowest-metallicity SFGs from Izotov et al. (2018a), the galaxy Little Cub (Hsyu et al. 2017), the galaxy J1234+3901 from Izotov et al. (2019a) and the H II region DDO 68#7 (Annibali et al. 2019) are shown by filled circles. SFGs with the highest O_{32} ratios in the range $\sim$ 20 - 40 (Izotov et al. 2017) are shown by asterisks. Samples of SFGs used for the He abundance determination (Izotov et al. 2014, and references therein) are shown by open circles. Grey dots represent SFGs at $z > 0.02$ from the SDSS, with the [O III]λ4363 emission line measured with an accuracy better than 20 per cent. The solid lines in **b)** and **c)** are linear fits to the data with log($R_{23} - a_0O_{32}$) $\leqslant$ 0.7 and log($R_{23} - a_1O_{32}$) $\leqslant$ 0.7, respectively, and excluding J1631+4426.